Influence of the preparation conditions of Pd-ZrO_2, PdAu-ZrO_2 nanoparticles decorated functionalised MWCNTs - electron spectroscopy study aided with the QUASES

B. Lesiak,[1,*] J. Zemek,[2] P. Jiricek[2]

[1]*Institute of Physical Chemistry, Polish Academy of Sciences, Kasprzaka 44/52, 01-224 Warszawa, Poland*

[2]*Institute of Physics, Academy of Sciences of the Czech Republic, 162-53 Prague 6, Cukrovarnicka 10, Czech Republic*

[*]Corresponding author: *e-mail: blesiak-orlowska@ichf.edu.pl*

Abstract

The Pd, PdAu and ZrO_2 nanoparticles decorated functionalised MWCNTs (f-MWCNTs) were reported as efficient catalysts of formic acid electro-oxidation. Evaluation of accurate surface parameters is of high importance since different preparation conditions influence the chemical, structural and catalytic properties. Chemical and structural properties of Pd and PdAu decorated ZrO_2/f-MWCNTs prepared using different procedures were analysed using X-ray photoelectron spectroscopy (XPS) aided with the Quantitative Analysis of Surfaces by Electron Spectroscopy (QUASES).

Methods using different reduction strength procedures, like $NaBH_4$ reducing agent at RT > a polyol microwave-assisted method (PMWA) using ethylene glycol and NaOH at 170 $^oC \approx$ NaOH in a high pressure microwave reactor (HPMWR) at 250 ^oC, were applied for decorating ZrO_2/f-MWCNTs with Pd and PdAu nanoparticles. ZrO_2 nanoparticles were attached *via* oxygen groups on the surface of the f-MWCNTs. Pd and PdAu nanoparticles were placed predominantly on ZrO_2 nanoparticles in $NaBH_4$ and HPMWR methods and in PMWA method on the surface of f-MWCNTs. Strong reducing procedure using $NaBH_4$ led to the smallest Pd nanoparticle size, Pd oxide content, PdO_x overlayer thickness, insignificant Pd-O-Zr phase and absence of PdC_x phase. Weaker reduction procedures (PMWA and HPMWR methods) provided a larger Pd and PdAu crystallites size, Pd oxide content, Pd oxide overlayer thickness, PdC_x (in Pd decorated catalyst) and significant amount of Pd-O-Zr intermetallic phase (in PdAu decorated samples). Formation of PdC_x phase resulted from carbon contaminations from glycol and/or MWCNTs substrate. Formation of significant content of Pd-O-Zr phase in PdAu decorated ZrO_2/f-MWCNTs in contrary to Pd decorated sample prepared by PMWA method could be justified by different electronic properties, *i.e.* alloy formation and smaller nanoparticles size. Treatment with a formic acid resulted in decreasing Pd oxide content, PdO_x overlayer thickness, size of ZrO_2, Pd and PdAu nanoparticles, accompanied by increasing ZrO_2 and Pd/PdAu nanoparticles surface coverage and density due to nanoparticles surface rearrangement increasing Pd coverage on ZrO_2.

Keywords: XPS; QUASES; Pd-ZrO_2/f-MWCNTs; PdAu-ZrO_2/f-MWCNTs; a high pressure microwave reactor (HPMWR); a polyol microwave-assisted method (PMWA).

Introduction

Carbon nanotubes (CNTs) are extensively studied due their unique physicochemical properties and possibility of tailoring these properties by functionalisation with different oxygen groups and decoration with nanoparticles of metal and metal oxides. Among these, metal and/or metal oxides decorated CNTs devoted a high interest due to their technological application in catalysis, bio/chemical sensoring, energy storage and production, individual electrical CNTs properties studies [1], *etc.* For a catalytic purpose, the metal (mainly Pd substituting Pt) and PdAu catalysts supported MWCNTs [2-13], and recently Pd-ZrO_2 on functionalised MWCNTs (f-MWCNTs) [14] were applied. These Pd and PdAu decorated f-MWCNTs catalysts of formic acid electro-oxidation (on an anode side) [9-13], prepared with the same metal loading (20 wt. %) using different methods, provided information on their higher catalytic activity exceeding the respective for Pt catalysts. The modified 20 wt. % Pd-ZrO_2/f-MWCNTs catalyst [14] showed slightly smaller catalytic activity due to a larger Pd nanoparticles size, however was shown to be more resistant for deactivation and sintering of Pd nanoparticles due to thermo-chemical treatment in oxygen and hydrogen [14]. This enhanced catalytic stability was attributed to oxidation of CO_{ad} on Pd to CO_2, *i.e.* "self-cleaning" mechanism, due to oxygen from the MWCNTs functional hydroxyl groups, -OH, oxygen vacancies in ZrO_2, ZrO_2 activation of water being decomposed into active oxygen radicals and modified adsorption properties [14].

Physicochemical and structural properties of deposited metal nanoparticles on carbon nanostructure catalysts depend significantly on the preparation method (metal loading, chemicals, pH), the support (its specific area and porosity) and support functionalisation (oxygen groups, *i.e.* hydroxyl, carbonyl, epoxy, carboxyl). A number of methods employed till now for preparation of Pd based functionalised MWCNTs new hybrid materials resulted in a wide variety of structural, electrochemical and catalytic properties [2-14]. These structural and electrochemical properties have been studied by the TEM, SEM, XRD, Raman

and FTIR, electron spectroscopy methods, cyclic voltammetry, chronoamperometry and in a fuel cell [2-14].

Alternative method for determining the surface structural parameters employs the X-ray photoelectron spectroscopy (XPS) aided with the QUASES (Quantitative Analysis of Surfaces by Electron Spectroscopy) procedure [15]. Basic theory of QUASES [16,17], application of the theory for description of the surface 3D nanostructure in-depth profiles and atomic surface coverage [18,19] and evaluation of the QUASES method accuracy [20] have been already published. This procedure was developed for describing the surface 3D nanostructure. For this purpose the XPS spectra and the inelastic background in the spectra vicinity are examined. The inelastic background varies when electrons travelling through a solid characterised by different in-depth profiles lose their kinetic energy (KE). The measured spectrum, $J(E,\Omega)$, of emitted electrons of energy E into the solid angle, Ω, is expressed as:

$$J(E,\Omega) = \int dE_o F(E_o,\Omega) \int f(x) G(E_o, x/\cos\theta; E) dx \,, \quad (1)$$

where $F(E_o,\Omega)$ is the flux density of photoelectrons excited from a single atom at energy E_o into the solid angle Ω, $f(x)$ is the concentration of atoms at depth x, θ is the emission angle with respect to the surface normal and the function G is the energy distribution of an electron as a function of its path length $x/\cos\theta$ travelled in a solid. QUASES evaluation proceeds by: (i) inelastic background removing (QUASES-Analyze), (ii) inelastic background removing using a standard (QUASES-Analyze) and (iii) modeling of spectrum from the standard to adjust the intensity and background to the respective spectrum from the investigated sample (QUASES-Generate). For these evaluations the in-depth profile, $f(x)$, should be assumed and then surface morphology parameters (atomic coverage, overlayer thickness, islands height, *etc.*) are determined. Available in-depth profiles are: (i) Buried Layer, *i.e.* spectrum of electrons emitted from a layer of a certain thickness and in-depth position, (ii) Islands Passive Substrate, *i.e.* spectrum of electrons emitted from an overlayer of atoms of certain coverage and thickness, (iii) Islands Active

Substrate, *i.e.* spectrum of electrons emitted from atoms of a substrate, (iv) Exponential Profile, *i.e.* increasing or decreasing with a depth and (v) Several Buried Layers, *i.e.* several thin layers at different depths and widths. Calculations require also transmission function of the analyser, geometry of analysis, investigated electron inelastic mean free path (IMFP) values, dependent on kinetic energy and material [21] and inelastic scattering cross-sections available in a software [22].

The purpose of this study performed by the XPS aided with QUASES was:

(i) evaluation of the chemical and structural properties of the 20 wt. % Pd-ZrO_2/f-MWCNTs and 10 wt. % Pd 10 wt. % Au-ZrO_2/f-MWCNTs catalysts,

(ii) investigation of influence of different reducing conditions during catalyst preparation (a high pressure microwave reactor - HPMWR at 250 ^oC in a presence of NaOH, a strong reducing agent $NaBH_4$ at room temperature (RT), a polyol microwave-assisted method - PMWA at 170 ^oC in a presence of ethylene glycol and NaOH) on the chemical and structural properties of 20 wt. % Pd-ZrO_2/f-MWCNTs catalyst,

(iii) investigation of the effect of a formic acid (FA) on the chemical and structural properties of 20 wt. % Pd-ZrO_2/f-MWCNTs and 10 wt. % Pd 10 wt. % Au-ZrO_2/f-MWCNTs catalysts prepared by PMWA method.

Experimental

Samples

The following samples, with notation and preparation conditions given below, were analysed:

f-MWCNTs – the functionalised MWCNTs, *i.e.* MWCNTs-$COONH_4$, prepared from the "as-received" MWCNTs (CNT CO., LTD., Korea) of average diameter size of 20 nm to 40 nm, where the "as-received" MWCNTs were treated in boiling concentrated (68%) HNO_3 under a reflux condenser for about 50 h at 120 ^oC to remove amorphous carbon, traces of catalysts and their support and oxidise, washed with deionised water, then with NH_4OH and again deionised water until stabilisation of filtrate pH (pH~7).

After such functionalisation the surface area increased from 177 m^2/g ("as-received" MWCNTs) to 254 m^2/g (f-MWCNTs).

ZrO_2/f-MWCNTs – 20 wt. % ZrO_2, 80 wt. % of f-MWCNTs prepared using a hydrothermal method by means of a microwave reactor. A mixture of MWCNTs-$COONH_4$, 0.05 M aqueous solution of ZrO_2 precursor, *i.e.* zirconyl chloride ($ZrOCl_2$) and an aqueous solution of 1 M NaOH (to pH=10) was heated in the reactor at a pressure of 55 bar, to a temperature of 250 ^oC for 30 minutes. Then, the sample was washed by distilled water and dried.

P1 (Pd-ZrO_2/f-MWCNTs HPMWR) - 20 wt. % Pd, 16 wt. % ZrO_2, 64 wt. % of f-MWCNTs prepared in a closed reactor using a mixture of adequate amount of MWCNT-$COONH_4$, 0.05 M aqueous solution of ZrO_2 precursor, *i.e.* zirconyl chloride ($ZrOCl_2$), solution of $PdCl_2$ (5 wt. % in 10% HCl, Sigma) and aqueous solution of 1 M NaOH (to adjust pH to 10) was heated in the reactor at a pressure of 55 bar to a temperature of 250 ^oC for 30 minutes. Then, the sample was washed in distilled water and dried.

P2 – (Pd-ZrO_2/f-MWCNTs $NaBH_4$) - 20 wt. % Pd, 16 wt. % ZrO_2, 64 wt. % of f-MWCNTs prepared in an open reactor from mixing water solution of ZrO_2/f-MWCNTs with $PdCl_2$ (5 wt. % in 10% HCl, Sigma) and 1M NaOH (to adjust pH to 10), slowly adding 1M solution of $NaBH_4$ at RT continuously mixing in ultrasonic bath (30 min.), after rinsed in water and acetone and dried at RT overnight.

P3 – (Pd-ZrO_2/f-MWCNTs PMWA) - 20 wt. % Pd, 16 wt. % ZrO_2, 64 wt. % of f-MWCNT prepared in an open reactor from ZrO_2/f-MWCNT dispersed in an excess of ethylene glycol to which an adequate amount of aqueous solution of $PdCl_2$ (5 wt. % in 10% HCl, Sigma) was added. Next, NaOH aqueous solution was added to the mixture to adjust the pH value to 7. The reaction mixture was kept in a microwave reactor at the temperature of 170˚C for 60 seconds. After the preparation the sample was rinsed with water and acetone and dried at room temperature.

$P3_{FA}$ – (Pd-ZrO_2/f-MWCNTs PMWA FA) - before the XPS measurements the sample P3 – (Pd-ZrO_2/f-MWCNTs PMWA) rinsed with FA for 15 minutes.

P4 – (PdAu-ZrO_2/f-MWCNTs PMWA) - 10 wt. % Pd, 10 wt. % Au, 16 wt. % ZrO_2, 64 wt. % of f-MWCNTs prepared in an open reactor from ZrO_2/f-MWCNT dispersed in an excess of ethylene glycol to which an adequate amount of aqueous solution of $PdCl_2$ (5 wt. % in 10% HCl, Sigma) and $AuCl_3$ (ACROS) was added. Next NaOH aqueous solution was added to the mixture to adjust the pH value to 7. The reaction mixture was kept in a microwave reactor at the temperature of 170˚C for 60 seconds. After preparation the sample was rinsed with water and acetone and dried at room temperature.

$P4_{FA}$ – (PdAu-ZrO_2/f-MWCNTs PMWA FA) - before the XPS measurements the sample P4 – (PdAu-ZrO_2/f-MWCNTs PMWA) rinsed with FA for 15 minutes.

Apparatus

The scanning transmission electron microscopy (STEM) and scanning electron microscopy (SEM) pictures were taken using a high resolution scanning electron microscope HITACHI S-5500 in a bright-field scanning transmission mode.

The XPS spectra were recorded in UHV using and ADES-400 spectrometer (VG Scientific, UK) equipped with a hemispherical analyser, a scanning electron gun (Kimball Physics, model EGG-3101) and X-ray excitation source. The XPS measurements were carried out using MgK_α radiation (hν=1253.6 eV). The wide scans XPS spectra and detailed C 1s, O 1s, Pd $3d_{5/2-3/2}$, Zr $3d_{5/2-3/2}$, Au $_{4f7/2-5/2}$ and N 1s XPS spectra were recorded with the pass energy E_p=100 eV and E_p=20 eV, respectively. The X-ray incidence angle was of 70^o and the photoelectrons emission angle was of α_{out} = 0^o, with respect to the surface normal.

Results and discussion

STEM

The STEM and SEM images showed ZrO_2 nanoparticles on the MWCNTs surface covering about 30 percent of their surface area (Fig. 1). Their distribution, generally homogeneous, indicated also larger agglomerates of these nanoparticles. The average size of ZrO_2 nanoparticles observed ranged from about 5 nm to 15 nm.

Quantitative analysis

The f-MWCNTs showed at the surface C, O and N, the sample ZrO_2/f-MWCNTs showed Zr, C and O, whereas the samples P1-P4 - the presence of Pd, Zr, C, O and traces of Si (P2). The atomic content at the surface was quantified from the peak areas after Tougaard-type background subtraction [23], assuming a model of homogeneous distribution of atoms at the surface, Scofield photoionisation cross-section, analyser transmission function and electron elastic scattering [24]. The quantitative evaluation proceeded using Pd 3d, Zr 3d, C 1s, O 1s and Si 2p spectra. For samples P1-P4 the area under Pd 3d spectra was evaluated from the fitting of the overlapping Pd 3d and Zr 3p spectra (Fig. 2) to the asymmetric Gaussian-Lorentzian GL(30) functions using XPSPeakfit4.1 software [25]. The results of the quantitative analysis were given in Table 1.

The highest content of Pd (close to the nominal resulting from the chemical synthesis, *i.e.* ca 20 wt. %) showed the samples prepared on f-MWCNTs using HPMWR (P1) and $NaBH_4$ (P2) with Zr content lower than the nominal of 16 wt. %, *i.e.* 9.9-11.1 wt. %. In Pd-ZrO_2/f-MWCNTs and PdAu-ZrO_2/f-MWCNTs samples prepared using PMWA method (P3, P4), also after rinsing with FA ($P3_{FA}$, $P4_{FA}$), the Pd content was lower (11.1-15.0 wt. %) than the nominal resulting from the chemical synthesis, whereas the content of Zr was close to the nominal, *i.e.* 16 wt. %. No significant changes in Pd content were

observed after treatment with FA. The content of Au in PdAu-ZrO_2/f-MWCNTs was lower by about 6-7 times than Pd after synthesis and FA.

The ratios of elemental surface content resulting from the quantitative analysis (Fig. 3) confirmed that the highest amount of Pd was observed for samples prepared using HPMWR (P1), whereas the presence of $NaBH_4$ led to its slight decrease (P2). Samples Pd-ZrO_2/MWCNTs and PdAu-ZrO_2/MWCNTs prepared using PMWA method (P3, P4) showed significantly smaller Pd/Zr ratio, *i.e.* P3 > P4. Treatment with FA did not lead to significant changes in Pd decorated sample, whereas in PdAu decorated sample led to increasing Pd/Zr and Pd/Au ratios and decreasing Au/Zr ratio. This indicated that in HPMWR and $NaBH_4$ using methods Pd decoration proceeded predominantly on ZrO_2 nanoparticles, whereas in PMWA method Pd decorates also the surface of f-MWCNTs. Previously reported results by the XRD for 10 wt. % Pd 10 wt. % Au decorated f-MWCNTs showed two AuPd phases of different nanoparticles size *i.e.* 3.8 nm (Au rich phase) and 5.3 nm (Pd rich phase), where reduction increased Pd content in PdAu nanoparticles, what was accompanied by slightly increasing size of Pd rich phase nanoparticles [12].

Chemical bonding of C and oxygen groups

The chemical state of C surface atoms was analysed from C 1s (sp^2, sp^3, hydroxyl – C-OH, carbonyl – C=O, carboxyl – C-OOH groups) XPS spectra (Fig. 4). The spectra were processed after subtracting Tougaard-type inelastic backgrounds, using the fitting to asymmetric Gaussian-Lorentzian GL(30) functions to the components of binding energy (BE) referring to different chemical states, according to the respective data from the literature [26-31]. All the C 1s spectra were calibrated to BE value of 284.4 eV. The difference between value of BE for the sp^2 and sp^3 component of 0.9 eV for amorphous carbon [29] and 0.8 eV for diamondlike films [30] have been previously reported. The difference of 1.3 eV was reported by Butenko at el. [28] for onionlike nanodiamonds, amorphous carbon film annealed above 1200 K [31]. In the present work this value was applied due to obtaining the best fitting results (Table 2). The BE typical for oxygen groups depend on their nature and as compiled by Butenko et al. [28] they are

shifted from the sp^2 towards higher BE values by 1.3-2.4 eV (C-OH), 2.6-3.5 eV (C=O) and 4.3-5.4 (C-OOH). The BE values applied for fitting being within the reported in the literature energy range and the atomic percent of different C chemical states are enclosed in Table 2.

The f-MWCNTs and ZrO_2, Pd and PdAu nanoparticle decorated f-MWCNTs indicated the presence of C sp^2, sp^3 hybridisations, oxygen groups like hydroxyl, carbonyl and carboxyl (Table 2, Fig. 4). Amount of C sp^3 ranges from 7.24 at. % to 10.76 at. % (P1-P4 samples) with the highest content for samples prepared by PMWA method and decreasing content after FA, *i.e.* from 10.76 at. % to 10.11 at. % (P3) and from 10.31 at. % to 9.49 at. % (P4). Respective value for f-MWCNTs and ZrO_2 decorated f-MWCNTs was 11.47 at. % and 10.53 at. %, respectively. The line shape of the first-derivative carbon KLL (KVV) spectrum sensitive to density of states (DOS) describing a linear combination from atoms involving sp^2 (graphite) and/or sp^3 (diamond) bonds can be used as a fingerprint of the carbon material (Fig. 5a) [32,33]. Changes in the carbon structure involve π DOS at about 280 eV, whereas changes in the region of about 240-260 eV reflect many-body correlation effects [34]. Parameter D, proposed by Laskovich et al. [35], defined as an energy difference between the maximum and minimum of the first-derivative C KLL spectra, may be applied for evaluating the C sp^2/sp^3 content from the linear interpolation of the respective values for diamond (100% of sp^3 bonds) and graphite (100% of sp^2 bonds). Literature reports the values of parameter D for diamond in a range of 13.0-16.4 eV and for graphite in a range of 21.1-23.1 eV [32-36], depending on the grain size and crystallinity and generally decreasing under oxygen impurities [36]. Parameter D evaluated from the first-derivative of the C KLL spectra assuming the value of 13.4 eV for diamond and 23.1 eV for graphite, ranges from 20-22 eV, indicating predominant C sp^2 hybridisations, although the shape of all the spectra shows different local disorder (Fig. 5a). Comparison of C sp^2/C sp^3 ratio resulting from the C 1s fitting (Table 2) and parameter D (C KLL spectra), *i.e.* from various information depths (Fig. 5b), indicated inhomogeneous distribution of sp^2/sp^3 bonds at the surface. Assuming a straight line approximation model (SLA) the information depth (ID) of a specified signal percentage (P), described by the equation: $ID(P)=\lambda\cos\alpha_{out}\ln(1/(1-P/100))$, where λ is

the electron IMFP and α_{out} is the emission angle with respect to the surface normal [37], the value of ID (P=45 %) is about 2.4 times smaller for the C KLL signal. Therefore, differences may be prescribed to a larger content of C sp^3 at the surface (f-MWCNTs, $NaBH_4$ preparation – P2, FA treatment – $P3_{FA}$, $P4_{FA}$) and a larger content of C sp^2 at the surface resulting from an overlayer of amorphous carbon due to preparation procedures (ZrO_2/f-MWCNTs, PMWA method – P3, P4). Results of C 1s fitting including the photoelectron inelastic loss on electrons forming π bonds, *i.e.* the ratio of intensity of C 1s π plasmon to C sp^2 and sp^3 bonds *versus* the π energy loss (Fig. 5c) are in agreement indicating increasing value of intensity of C 1s π plasmon to C sp^2 and sp^3 and π energy loss is attributed to a larger C sp^2 content [38].

Decoration of f-MWCNTs with 20 wt. % ZrO_2 nanoparticles led to decrease of content of functional groups, like hydroxyl, carbonyl and carboxyl, from the MWCNTs surface (Table 2, Fig. 6). Further decoration of ZrO_2/f-MWCNTs with Pd and PdAu nanoparticles and treatment with FA led to increasing content of oxygen groups, more significantly in PMWA method than in HPMWR and method using $NaBH_4$. Modification of oxygen groups (C-OH, C=O, C-OOH) content depended on the preparation method applying different temperatures, where oxygen groups also underwent thermal decomposition at various temperatures, *i.e.* 150 ^oC (C-OOH) and above 400 ^oC (C-OH and C=O) [39].

Chemical bonding of Zr

The chemical state of Zr was analysed from Zr $3d_{5/2-3/2}$ spectra submitted to Tougaard's inelastic background subtraction procedure and fitting to Gaussian-Lorentzian GL(30) function. The features of the Zr 3d spectra, like the BE of Zr $3d_{5/2}$ and differences between BE of Zr $3d_{5/2}$ and Zr $3d_{3/2}$ doublet (ΔBE $Zr_{5/2-3/2}$), so called Zr 3d doublet splitting, were evaluated (Table 3). The Zr 3d spectrum of ZrO_2 indicated the BE of Zr $3d_{5/2}$ at 182.6 eV, according to the literature data [26]. The respective spectrum recorded from the ZrO_2/f-MWCNTs was shifted towards the higher BE values by 0.5 eV, *i.e.* to 183.1 eV (Table 3). This was accompanied by decreasing number of C=O and C-OOH groups (Table 2, Fig. 6) and

decreasing Zr 3d doublet splitting (Table 3), indicating formation of bond between ZrO_2 nanoparticles and functional groups of the MWCNTs, reported elsewhere [14].

Further decoration of ZrO_2/f-MWCNTs with Pd and PdAu nanoparticles provided the Zr $3d_{5/2}$ BE shift towards higher energies (183.0±0.1 eV) with respect to this value for ZrO_2 (182.6 eV), suggesting formation of the chemical bond of Pd and PdAu nanopartcles *via* oxygen groups and/or ZrO_2. Value of this shift depended on reducing conditions Weak PMWA reducing conditions in ethylene glycol (P3-P4), provided no shift. The HPMWR and $NaBH_4$ reducing conditions provided a shift from 183.1 eV to 183.7 eV (P1) and to 183.4 eV (P2), respectively. Value of Zr 3d doublet splitting decreased from 2.40 eV (ZrO_2) to 2.34-2.38 eV (P1-P4) confirming interaction of ZrO_2 with Pd and PdAu, probably *via* oxides and/or oxygen groups at the surface of functionalised MWCNTs. Similar decrease of Zr 3d doublet splitting value from 2.4 eV to 2.2 eV was reported for $PdZrO_2$ catalysts prepared using different procedures and was interpreted as resulting from formation of Zr-O-Pd chemical state [40]. Formation of an intermetallic compound, such as $PdOZrO_x$, was confirmed elsewhere by the EPMA microanalysis [41]. Treatment with a formic acid of P3 and P4 samples does not provide significant differences in the Zr $3d_{5/2}$ BE value and Zr 3d doublet splitting, indicating no significant influence of reduction with FA on Zr-O-Pd chemical state.

Chemical bonding of Pd

Chemical state of Pd was investigated from the Pd $3d_{5/2-3/2}$ (and overlapping Zr 3p) spectra after subtracting Tougaard-type inelastic backgrounds and fitting asymmetric Gaussian-Lorentzian GL(30) functions to the components referring to different possible chemical states [26,42,43]. Results of fitting of the Pd 3d spectrum overlapping with Zr 3p spectrum (Fig. 2 and 4), considering metallic Pd, PdO, PdO_2 [26,42], PdC_x [43,44] and Pd attached *via* oxides and/or oxygen groups [45], and values of the Zr $3d_{5/2}$ BE shift and Zr 3d doublet splitting were shown in Table 3. The values of BE for Pd $3d_{5/2}$ spectra in PdO and

PdO_2 resulting from the fitting (Table 3) were in the range of values reported in the literature, *i.e.* 336.3-337.2 eV (PdO) and 337.9-339.3 eV (PdO_2) [42 and references within]. Values of Zr 3d doublet splitting decreasing to 2.34 eV would suggest interaction of Zr with $Pd[OC(O)CH_3]_2$ [45]) and formation of Pd-zirconia phase *via* oxygen groups of f-MWCNTs.

Sample prepared by the HPMWR method (P1) showed the highest content of Pd oxides and Pd-zirconia intermetallic phase (Table 3, Fig. 7). Conditions of $NaBH_4$ (P2) led to the least content of Pd oxides and insignificant Pd-zirconia intermetallic phase. The PMWA method led to formation of Pd oxides in Pd decorated samples, whereas in PdAu decorated samples Pd oxide significant content of intermetallic Pd-zirconia phase was observed. In HPMWR method the BE value for PdO (336.6 eV) indicated surface oxide phase, whereas in PMWA method bulk PdO was observed at 337.0±0.1 eV [42]. Formation of PdC_x phase due to carbon contaminations from ethylene glycol and/or MWCNTs substrate proceeded in Pd decorated samples prepared by HPMWR and PMWA methods. Similar results were reported previously for Pd decorated f-MWCNTs prepared using the same methods [13]. Reduction with hydrogen resulted also in formation of PdC_x in Pd decorated f-MWCNTs [11], with no similar effect in PdAu decorated f-MWCNTs [12]. Formation of Pd-O-Zr phase in PdAu decorated ZrO_2/f-MWCNTs in contrary to Pd decorated samples prepared by PMWA method could be justified by different electronic properties due to alloy formation and decreasing of the nanoparticle size.

The BE values for metallic Pd vary for different preparation procedures (Table 3). This BE shift was interpreted as resulting from the initial and final state effects. As reported by Wertheim et al. [46] for Pd clusters with decreasing cluster size the unfilled 4d band valence band spectra show the d-band narrowing and a positive shift of the binding energies. The BE values of Pd $3d_{5/2}$ spectra indicated the largest Pd nanoparticles for preparation using HPMWR method (P1), whereas preparation by PMWA method (P3, P4) and FA treatment ($P3_{FA}$,$P4_{FA}$) led to smaller nanoparticle sizes. The smallest nanoparticle size was observed for a sample prepared using $NaBH_4$ reducing agent.

Chemical bonding of Au

The chemical state of Au in P4 and $P4_{FA}$ samples was analysed from Au $4f_{7/2-5/2}$ spectra submitted to Tougaard's inelastic background subtraction procedure and fitting to Gaussian-Lorentzian GL(30) function. The BE values of Au $4f_{7/2}$, the Au $4f_{7/2-5/2}$ doublet splitting and the FWHM values were analysed (Table 3). The Au $4f_{7/2}$ BE values for PdAu-ZrO_2/f-MWCNTs being 83.6 eV (after synthesis – P4) and 83.8 eV (treatment with FA – $P4_{FA}$) (Table 3) differ from the respective values for metallic Pd, *i.e.* BE=84.0 eV [26], due to the presence of PdAu phase reported elsewhere for the same preparation method [12]. The reported values of Au $4f_{7/2-5/2}$ doublet splitting, *i.e.* 3.60 eV (P4) and 3.57 eV ($P4_{FA}$), and FWHM, *i.e.* 2.26 eV (P4) to 2.32 eV ($P4_{FA}$), being smaller than the respective values for a bulk Au, *i.e.* Au $4f_{7/2-5/2}$ splitting of 3.67 eV [26], result from nanoparticles formation. As reported previously for Au $4f_{7/2}$ spectrum [47], decreasing of nanoparticle size is accompanied by increasing values of BE, with increasing values of Au $4f_{7/2-5/2}$ splitting and FWHM. Formic acid treatment led to increasing value of BE, and negligible changes of Au $4f_{7/2}$ doublet splitting and FWHM values. Results reported previously for a polyol microwave-assisted prepared 20 wt. % PdAu nanoparticles on functionalised MWCNTs confirmed the existence of two PdAu phases, *i.e.* Pd rich and Au rich, where reduction at 200 ^{o}C in hydrogen led only to modification of both phases compositions [12], what could explain the BE shift reported in the present work of PdAu/ZrO_2/MWCNTs obtained after FA. Otherwise, no significant modifications of lattice parameters and nanoparticle size were observed [12].

Surface morphology

Surface morphology of Pd/PdAu-ZrO2 decorated f-MWCNTs was evaluated using Pd 4p, Au 4f and Zr 3d XPS spectra (including the inelastic background in the spectra vicinity) recorded from the investigated samples and the respective spectra from a clean metallic Pd, Au and ZrO_2 by the QUASES-Analyze procedure [15]. For evaluating the surface coverage of different nanoparticles the Buried Layer Model with respective standards (ZrO_2, Pd, Au) was applied (Fig. 8). For determining the nanoparticles

height the Passive Substrate Model accounting for the evaluated previously coverage was used (Table 4). Evaluation accounted for an analyser transmission function [48], universal cross-section for inelastic scattering implemented into the software and the inelastic mean free path values by Tanuma et al. [21] (Table 4). The density of clusters per cm^2 (n), assuming a spherical cluster size, was evaluated from the equation [19]:

$$n = \frac{f_1}{\pi R^2} x\, 10^{16} \quad , \tag{1}$$

where πR^2 is the projected area of a given spherical cluster, R is the radius in Å and f_1 is nanoparticles surface coverage. The thickness of PdO_x overlayer on Pd, X_{PdO}, was evaluated according to the equation:

$$X_{PdO} = R - R\sqrt[3]{\frac{A}{1+A}}, \tag{2}$$

where $A = \frac{N_{Pd} M_{Pd} \rho_{PdO}}{N_{PdO} M_{PdO} \rho_{Pd}}$,

and R is the diameter of Pd/PdO_x nanoparticle evaluated from the QUASES, N_{Pd} and N_{PdO} are atomic percent of Pd and PdO, M_{Pd} (106.42 g mol^{-1}) and M_{PdO} (122.42 g mol^{-1}) are molar mass of Pd and PdO, ρ_{Pd} (12.023 g cm^{-3}) and ρ_{PdO} (8.3 g cm^{-3}) are the densities, respectively.

The values of surface coverage of ZrO_2, Pd and Au nanoparticles were shown in Fig. 8. The exemplary adjustment of the spectra including the inelastic background to the respective spectra recorded from the clean standard for evaluating the ZrO_2, Pd and Au nanoparticle size were shown in Fig. 9, whereas the values of ZrO_2, Pd, Au nanoparticle size and density per unit area (Eq(2)) and PdO_x overlayer thickness (Eq (1)) were listed in Table 4. The ZrO_2/f-MWCNTs sample indicated the ZrO_2 nanoparticles of 13.7 nm diameter covering about 30 % of the f-MWCNTs area (Table 4, Fig. 1 and 8). Further decoration of ZrO_2/f-MWCNTs with Pd by HPMWR method (P1) and using $NaBH_4$ (P2) led to

significant decrease of ZrO_2 coverage due to deposition of Pd nanoparticles on ZrO_2. In samples prepared by the PMWA method (P3, P4) the coverage of ZrO_2 remained similar to that for ZrO_2/f-MWCNTs, indicating precipitation of Pd and PdAu nanoparticles on the surface of f-MWCNTs. Treatment of samples P3 and P4 with FA led to significant increase of ZrO_2 coverage, slight increase of Pd and PdAu coverage and decrease of all nanoparticle size (Table 4, Fig. 8). Different conditions of preparation did not lead to significant differences in ZrO_2 nanoparticle size (12.3-14.0 nm) in contrary to Pd nanoparticles (6.9-16.1 nm). Conditions of HPMWR provided a larger size of Pd nanoparticles (16.1 nm) than conditions using PMWA method (9.4 nm) and $NaBH_4$ (6.9 nm). The largest thickness of PdO_x overlayer was observed for sample prepared in HPMWR conditions (2.16 nm) decreasing for preparation conditions in $NaBH_4$ to 0.16 nm. The PMWA conditions led to an intermediate value of Pd oxide overlayer thickness (0.32-0.35 nm), decreasing after FA (0.24-0.29 nm). However, the estimation applying Eq. (2) led to significantly underestimated values of overlayer thickness. The QUASES analysis indicated decrease of Pd and PdAu nanoparticle size after FA, *i.e.* from 9.4 nm to 8.2 nm (Pd) and from 9.5 nm to 8.6 nm (PdAu) due to reduction of Pd oxides (Table 3).

Previously reported results for Pd-ZrO_2/f-MWCNTs prepared by the PMWA method on Pd nanoparticle size, *i.e.* 8 nm (XRD) and 6-8 nm (HR-TEM) [14], are consistent with results obtained in the present work, *i.e.* 9.4 nm (QUASES). The ZrO_2 nanoparticle diameters (14.0 nm) were larger than previously reported, *i.e.* 8-10 nm (HR-TEM) and 4.4 nm (XRD) [14]. Discrepancies between evaluation by the HR-TEM and XRD arose from the sensitivity of methods for distinguishing amorphous ZrO_2 nanoparticles. Also, the QUASES procedure does not account for electron elastic scattering effect, which for rough surfaces modifies the signal intensity leading to an evaluation error of about several percent [49]. The size of PdAu nanoparticles obtained by the QUASES in PdAu-ZrO_2/f-MWCNTs (PMWA), *i.e.* 5.5 nm (Table 4) was comparable to the value obtained previously for PdAu/f-MWCNTs (PMWA method), *i.e.* 5.4 nm (TEM) and 3.9 nm for Au rich phase and 5.2 nm for Pd rich phase (XRD) [12]. The size of Pd nanoparticles decorating ZrO_2/f-MWCNTs obtained using HPMWR, $NaBH_4$ and PMWA

methods was larger than this obtained using the respective methods on the f-MWCNTs, *i.e.* 16.1 nm, 6.9 nm and 9.4 nm (QUASES) and 4.4 nm, 3.28 nm and 7.36 nm (XRD and XPS) [13].

The systematic error due to the application of the QUASES method resulted from: (i) samples surface roughness, (ii) systematic error in the values of the input parameters, *i.e.* the inelastic mean free path (IMFP), universal differential cross section, (iii) assumptions of the model not accounting for the interface between metallic nanoparticles and oxide overlayer. However, the largest contribution to the error in the results obtained by the QUASES is expected due to neglecting electron elastic scattering, where recent results [49] reported a significant influence of surface roughness on the photoelectron signal intensity.

Conclusions

Preparation conditions using various reduction procedures provided Pd, PdAu and ZrO_2 decorated f-MWCNTs samples of different chemical and structural properties. Conditions in HPMWR led to Pd nanoparticles situated predominantly on ZrO_2, largest Pd nanoparticle size with a thickest PdO_x overlayer, PdC_x phase and significant Pd-zirconia intermetallic phase, confirmed by the BE shift of Zr $3d_{5/2}$, Zr 3d doublet splitting. Conditions of PMWA method provided smaller Pd and PdAu nanoparticles situated predominantly on the surface of f-MWCNTs, less significant PdO_x overlayer thickness. Formation of PdC_x phase was observed in Pd decorated samples prepared by weak reduction methods (HPMWR and PMWA). No PdC_x phase was observed at PdAu decorated samples. Formation of significant content of Pd-zirconia intermetallic phase was observed in Pd decorated samples prepared by HPMWR method and in PdAu decorated samples prepared by PMWA method. Preparation using $NaBH_4$ led to Pd nanoparticles deposited predominantly on ZrO_2, the smallest Pd nanoparticles size, Pd oxide content, PdO_x overlayer thickness and insignificant Pd-zirconia intermetallic phase present.

Reduction in FA of Pd and PdAu decorated ZrO_2/f-MWCNTs samples provided decreasing Pd, PdAu and ZrO_2 nanoparticle size, increasing nanoparticles surface coverage due Pd oxides and functional groups reduction.

Method of XPS spectra analysis using the QUASES provided information on surface morphology, like nanoparticle surface coverage and size. The XPS aided with the QUASES may be applied as a complementary tool for determining the surface structural parameters.

Acknowledgments

The authors would like to thank to dr L. Stobinski (Institute of Physical Chemistry, Polish Academy of Sciences, Faculty of Chemical and Processing Engineering, Warsaw University of Technology), dr A. Malolepszy and dr M. Mazurkiewicz (Faculty of Chemical and Processing Engineering, Warsaw University of Technology) for sample preparation and performing the STEM and SEM pictures. Support by the Ministry of Education, Youth and Sports of the Czech Republic (Grant LM2015088) (J.Z., P.J.) is highly appreciated.

References

[1] Y.F. Hsiou, Y. J. Yang, L. Stobinski, W. Kuo. C.D. Chen, *Appl. Phys. Lett.* **2004**, *84*, 984.

[2] W.M. Daoush, T. Imae, *J. Mat. Research* **2012**, *27*, 1680.

[3] Y. Kuang, B. Wu, D. Hu, X. Zhang, J. Chen, *J. Solid State Electrochem.* **2012**, *16*, 759.

[4] Y.N. Jeonga, M.Y. Choi, H.C. Choi, *Electrochimica Acta* 2012, *60*, 78.

[5] Ch.T. Hsieh, Y.Y. Liu, Y.Sh. Cheng, W.Y. Chen, *Electrochimica Acta* 2011, *56*, 6336.

[6] H. Li, L. Han, J. Cooper-Whitea, I. Kim, *Green Chem.* **2012,** *14*, 14.

[7] Z.Y. Sun, Z. Li, Ch.L. Huang, Y.F. Zhao, H.G. Zhang, R. Tao, Z.M. Liu, *Carbon* **2011**, *9*, 4376.

[8] T. Maiyalagan, A. Bakr, A. Nassr, T.O. Alaje, M. Bron, K. Scott, *J. Power Sources* **2012**, *211*, 147.

[9] A. Mikolajczuk, A. Borodzinski, L. Stobinski, P. Kedzierzawski, B. Lesiak, L. Kövér, J. Tóth, H.M. Lin HM, *Phys. Status Solidi (b)* **2010**, *247*, 3063.

[10] A. Mikolajczuk, A. Borodzinski, L. Stobinski, P. Kedzierzawski, B. Lesiak, L. Kövér, L. Tóth, H.M. Lin, *Phys. Status Solidi (b)* **2010**, *247*, 2717.

[11] M. Mazurkiewicz, A. Malolepszy, A. Mikolajczuk, L. Stobinski, A. Borodzinski, B. Lesiak, J. Zemek, P. Jiricek, *Phys. Status Solidi (b)* **2011**, *248*, 2516.

[12] A. Malolepszy, M. Mazurkiewicz, A. Mikolajczuk, L. Stobinski, A. Borodzinski, B. Mierzwa, B. Lesiak, J. Zemek, P. Jiricek, *Phys. Status Solidi (c*) **2011**, *8*, 3195.

[13] M. Mazurkiewicz, A. Malolepszy, B. Lesiak, L. Stobinski, B. Mierzwa, A. Mikolajczuk-Zychora, K. Juchniewicz, A. Borodzinski, J. Zemek, P. Jiricek, *Appl. Surf. Sci*.387 (2016) 929.

[14] A. Malolepszy, M. Mazurkiewicz, L. Stobinski, B. Lesiak, L. Kövér, J. Tóth , B. Mierzwa, A. Borodzinski, F. Nitze, Th. Wågberg, *Int. J. Hydrogen Energy* **2015**, *40*, 16724.

[15] S. Tougaard, *QUASES: Software Packet for Quantitative XPS/AES of Surface Nano-Structures by Inelastic Peak Shape Analysis*, Version 5.1, 1994-2011 QUASES Tougaard Inc.; http://.www.quases.com.

[16] S. Tougaard, *Surf. Interface Anal.* **1988**, *11*, 453.

[17] S. Tougaard, *J. Vac. Sci. Technol.* A **1988,** *14*, 1415.

[18] L. Cattin, S. Tougaard, N. Stephant, S. Morsli, J.C. Bernède, *Gold Bull.* **2011**, *44*, 199.

[19] S.H. Hajati, V. Zaporojtchenko, F. Faupel, S. Tougaard, *Surf. Sci.* **2007**, *601*, 3261.

[20] S. Tougaard, *Surf. Interface Anal.* **1998**, *26*, 249.

[21] S. Tanuma, C.J. Powell, D.R. Penn, *Surf. Interface Anal.* **1994**, *21*, 165.

[22] S. Tougaard, *Surf. Interface Anal.* **1997**, *25*, 137.

[23] S. Tougaard, *Background analysis of XPS/AES. QUASES Simple Background*, Ver. 2.2, Copyright **1994-2001**; http://www.tougaard.com.

[24] M. Mohai, *Surf. Interface Anal.* **2004**, *36*, 828; M. Mohai, *Multimodel X-ray photoelectron spectroscopy quantification program for 32-bit Windows, XPS MultiQuant*, ver. 7, **1999-2001**.

[25] R.W.M. Kwok, *XPS Peak Fitting Program for WIN95/98 XPSPEAK*, Version 4.1, Department of Chemistry, The Chinese University of Hong Kong, rmkwok@cuhk.edu.hk; http://www.uksaf.org/software.html, XPSPEAK4.1.

[26] C.D. Wagner, A.V. Naumkin, A. Kraut-Vass, J.W. Allison, C.J. Powell, J.R. Rumble, Jr., *NIST X-ray Photoelectron Database*, NIST SRD 20, ver. 3.5, online, PC.

[27] S. Kundu, Y. Wang, W. Xia, M. Muhler, *J. Phys. Chem. C* **2008**, *112*, 16869.

[28] Yu.V. Butenko, S. Krishnamurthy, A.K. Chakraborty, V.L. Kuznetsov, V.R. Dhanak, M.R.C. Hunt, L. Šiller, *Phys. Rev. B* **2005**, *71*, 075420.

[29] R. Haerle, E. Riedo, A. Pasquarello, A. Baldereschi, *Phys. Rev. B* **2002,** *65*, 045101.

[30] P. Mérel, M. Tabbal, M. Chaker, S. Moisa, J. Margot, *Appl. Surf. Sci.* **1998**, *136*, 105.

[31] J. Díaz, G. Paolicelli, S. Ferrer, F. Comin, *Phys. Rev. B* **1996**, *54*, 8064.

[32] S. Kaciulis, A. Mezzi, P. Calvani, D.M. Trucchi, *Surf. Interface Anal.* **2013**, *46*, 966.

[33] L. Calliari, *Diamond Rel. Mat.* **2005**, *14*, 1232.

[34] H.J. Steffen, C.D. Roux, D. Marton, J.W. Rabalais, *Phys. Rev. B* **1991**, *44*, 3981.

[35] J.C. Laskovich, S. Scaglione, *Appl. Surf. Sci.* **1994,** *78*, 17.

[36] B. Lesiak, J. Zemek, J. Houdkova, A. Kromka, A. Jóźwik, *Anal. Sci.* **2010**, *26*, 217.

[37] A. Jablonski, C.J. Powell, *J. Vac. Sci. Technol A* **2009**, *27*, 253.

[38] V.N. Vasilets, A. Hirose, Q. Yang, A. Singh, R. Sammynaiken, M. Foursa, Y.M. Shulga, *Appl. Phys. A* **2004**, *79*, 2079.

[39] L. Stobinski, B. Lesiak, J. Zemek, P. Jiricek, Appl. Surf. Sci. 258 (2012) 7912.

[40] Y. Matsumura, M. Okumura, Y. Usami, K. Kagawa, H. Yamashit, M. Anpo, M. Haruta, *Cat. Let.* **1997**, *44*, 189.

[41] C.D. Qin, CC. Yu, D.H.L. Ng, L.C. Lim, M.O.Lai, *Mat. Let.* **1996**, *26*, 17.

[42] L.S. Kibis, A.I. Titkov, A.I. Stadnichenko, S.V. Koscheev, A.I. Boronin, *Appl. Surf. Sci.* **2009**, *255*, 9248.

[43] G. Mattogno, G. Polsonetti, G.R. Tauszik, *J. Electron Spectrosc. Rel. Penom.* **1978**, *14*, 237.

[44] A.V. Matveev, V.V. Kaichev, A.A. Saraev, V.V. Gorodetskii, A. Knop-Gericke, V.I. Bukhtiyarov, B.E. Nieuwenhuys, *Cat. Today* **2015**, 2*44*, 29.

[45] O. Balmes, A. Resta, D. Wermeille, R. Felici, M.E. Messing, K. Deppert, Z. Liu, M.E. Grass, H. Bluhm, R. van Rijn, J.W.M. Frenken, R. Westerström, S. Blomberg, J. Gustafson, J.N. Andersen, E. Lundgren, *Phys. Chem. Chem. Phys.* **2012**, *14*, 4796.

[46] G.K. Wertheim, S.B. DiCenzo, D.N.E. Buchnan, *Phys. Rev. B* **1986**, *33*, 5384.

[47] L. Calliari, G. Speranza, L. Minati, V. Micheli, A. Baranov, S. Fanchenko, *Appl. Surf. Sci.* **2008**, *255*, 2214.

[48] P. Jiricek, *Czech J. Phys.* **1994**, *44*, 261.

[49] J. Zemek, *Anal. Sci.* **2010**, *26*, 177.

Table 1. The results of surface quantitative analysis.

Sample	Element atomic %						Element weight %					
	Pd	Zr	Au	O	C	N	Pd	Zr	Au	O	C	N
f-MWCNTs	-	-	-	9.3	89.2	1.5	-	-	-	12.0	86.3	1.7
ZrO_2/f-MWCNTs	-	3.3	-	13.4	83.3	-	-	19.7	-	14.2	66.1	-
P1	4.2	2.0	-	20.2	73.6	-	24.2	9.9	-	17.7	48.2	-
P2*	4.7	2.3	-	20.6	72.4	-	26.3	11.1	-	17.2	45.4	-
P3	2.4	2.9	-	14.2	80.5	-	15.0	15.4	-	13.2	56.4	-
$P3_{FA}$	2.2	2.7	-	18.5	76.6	-	14.0	14.4	-	17.4	54.2	-
P4	1.8	3.1	0.3	15.8	79.0	-	11.1	16.3	3.3	14.6	54.7	-
$P4_{FA}$	2.1	3.4	0.3	14.5	79.7	-	12.8	17.2	3.1	13.1	53.8	-

*Si – 4.4 at% corrected

Table 2. The atomic content of carbon and oxygen groups.

Sample	C chemical state – C 1s				
	C sp^2 BE=284.4±0.1 eV	C sp^3 BE=285.7±0.1 eV	C-OH BE=286.7±0.1 eV	C=O BE=287.9±0.1 eV	C-OOH BE=288.9±0.1 eV
	at. %	at. %	at. %	at. %	at. %
f-MWCNTs	65.87	11.47	6.38	3.50	1.98
ZrO_2/f-MWCNTs	63.16	10.53	5.46	2.78	1.37
P1	56.75	7.24	5.79	1.29	2.42
P2	54.79	8.81	4.74	2.65	1.41
P3	59.25	10.76	6.17	2.86	1.46
$P3_{FA}$	56.46	10.11	5.59	2.95	1.49
P4	59.06	10.31	5.66	3.35	0.62
$P4_{FA}$	59.53	9.49	6.14	2.90	1.64

Table 3. The atomic content of Pd chemical states, BE values of Zr $3d_{5/2}$, Au $4f_{7/2}$, Zr $3d_{5/2}$ and $Zr_{5/2-3/2}$ doublet splitting.

Sample	Pd chemical state – Pd $3d_{5/2}$							Zr $3d_{5/2}$		Au $4f_{7/2}$
	PdC_x BE=BE_{Pd} +0.6 eV	Pd met		PdO		PdO_2 BE=338.0 ±0.1 eV	Pd[OC(O) $CH_3]_2$-ZrO_2 339.9±0.1 eV	BE (eV)	ΔBE $Zr_{5/2-3/2}$	
	at. %	BE (eV)	at. %	BE (eV)	at. %	at. %				
ZrO_2	-	-	-	-	-	-	-	182.6	2.40	-
ZrO_2/f-MWCNTs	-	-	-	-	-	-	-	183.1	2.36	-
P1	0.32	335.10	1.27	336.4	1.73	0.46	**0.42**	183.7	**2.34**	-
P2	-	335.62	4.27	-	-	0.39	0.04	183.4	2.38	-
P3	0.37	335.33	1.78	337.0±0.1	0.06	0.19	-	183.0±0.1	2.37	-
$P3_{FA}$	0.61	335.24	1.42	337.0±0.1	0.02	0.15	-	183.0±0.1	2.37	-
P4	-	335.45	1.36	337.0±0.1	0.06	0.15	**0.23**	183.0±0.1	**2.34**	83.6
$P4_{FA}$	-	335.45	1.59	337.0±0.1	0.12	0.11	**0.28**	183.0±0.1	**2.34**	83.8

Table 4. The morphology parameters resulting from the QUASES structural analysis.

Sample	Morphology parameters resulting from the QUASES						XPS
	Zr 3d KE=1073 eV IMFP (ZrO_2)=1.97 nm		Pd 4p KE=1200 eV IMFP (Pd)=1.60 nm		Au 4f KE=1170 eV IMFP (Au)=1.38 nm		PdO_x overlayer thickness (nm)
	ZrO_2 particle height (nm)	ZrO_2 particle density x10^{12} cm^{-1}	Pd/PdAu particle height (nm)	Pd/PdAu particle density x10^{12} cm^{-1}	PdAu particle height (nm)	PdAu particle density x10^{12} cm^{-1}	
ZrO_2 /f-MWCNTs	**13.7**	19.9	-				-
P1	**13.6**	9.2	**16.1**	3.1			2.16
P2	**13.9**	10.2	**6.9**	13.6			0.16
P3	**14.0**	18.4	**9.4**	8.4			0.32
$P3_{FA}$	**12.3**	32.8	**8.2**	14.0			0.24
P4	**13.9**	15.5	**9.5**	6.8	5.5	1.7	0.35
$P4_{FA}$	**13.6**	36.1	**8.6**	16.7	6.0	2.8	0.29

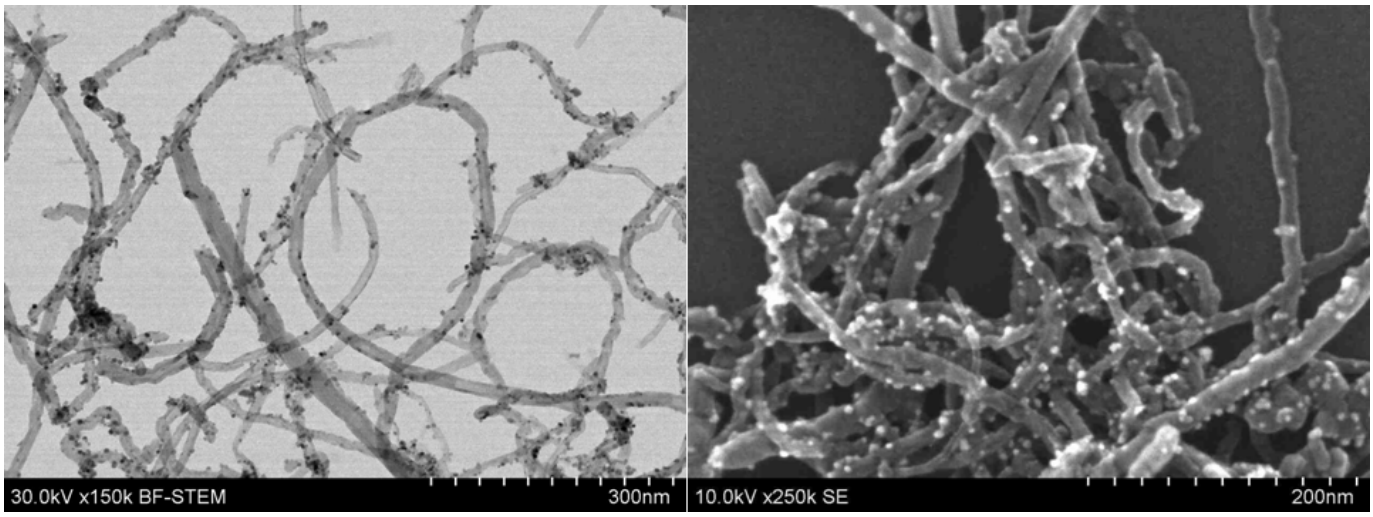

Fig. 1. Pictures of (a) STEM and (b) SEM presenting the functionalised MWCNTs decorated with 20 wt. % of ZrO_2 nanoparticles.

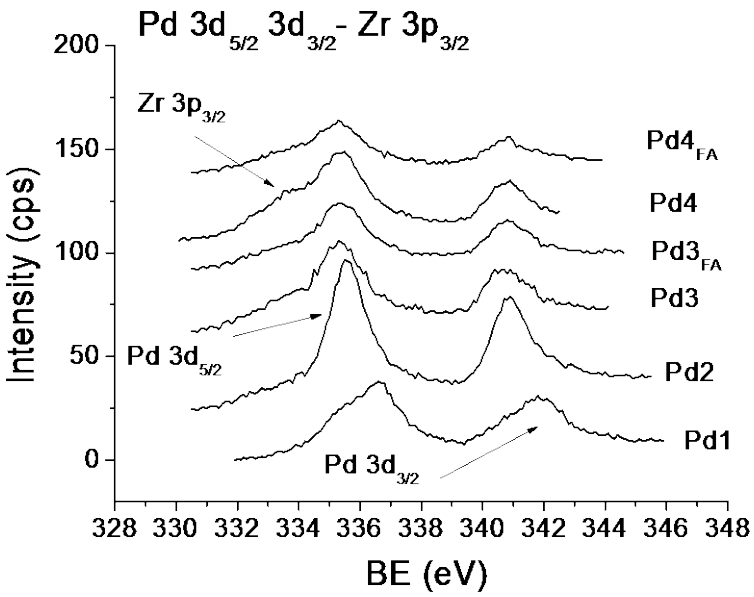

Fig. 2. Comparison of XPS Pd 3d-Zr 3p spectra recorded from the investigated samples. The sample notation is taken from the section 2.1.

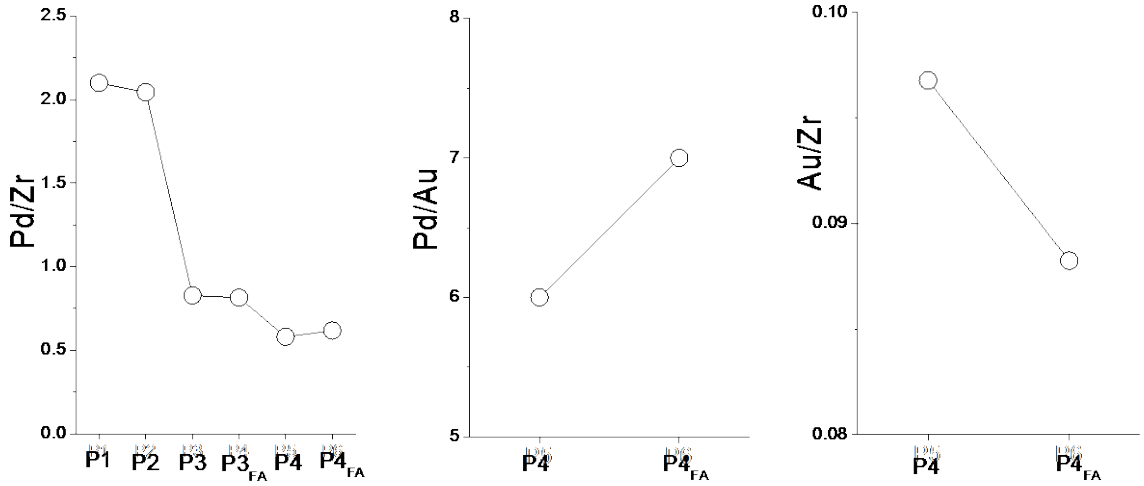

Fig. 3. The atomic concentration ratio of Pd/Zr, Pd/Au and Au/Zr content resulting from the quantitative analysis (Table 1). The sample notation is taken from the section 2.1.

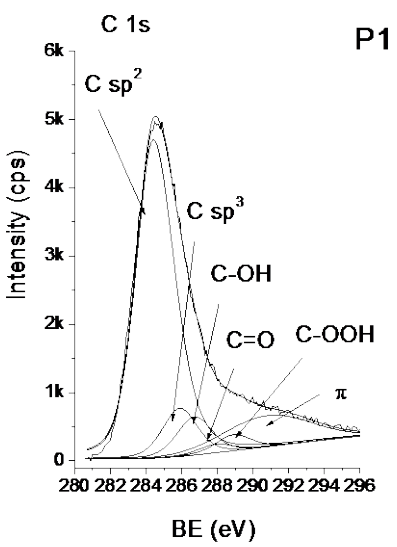

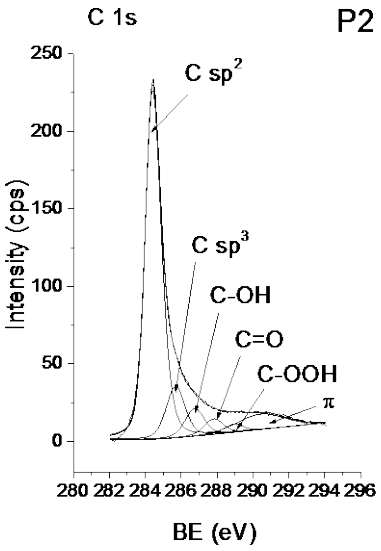

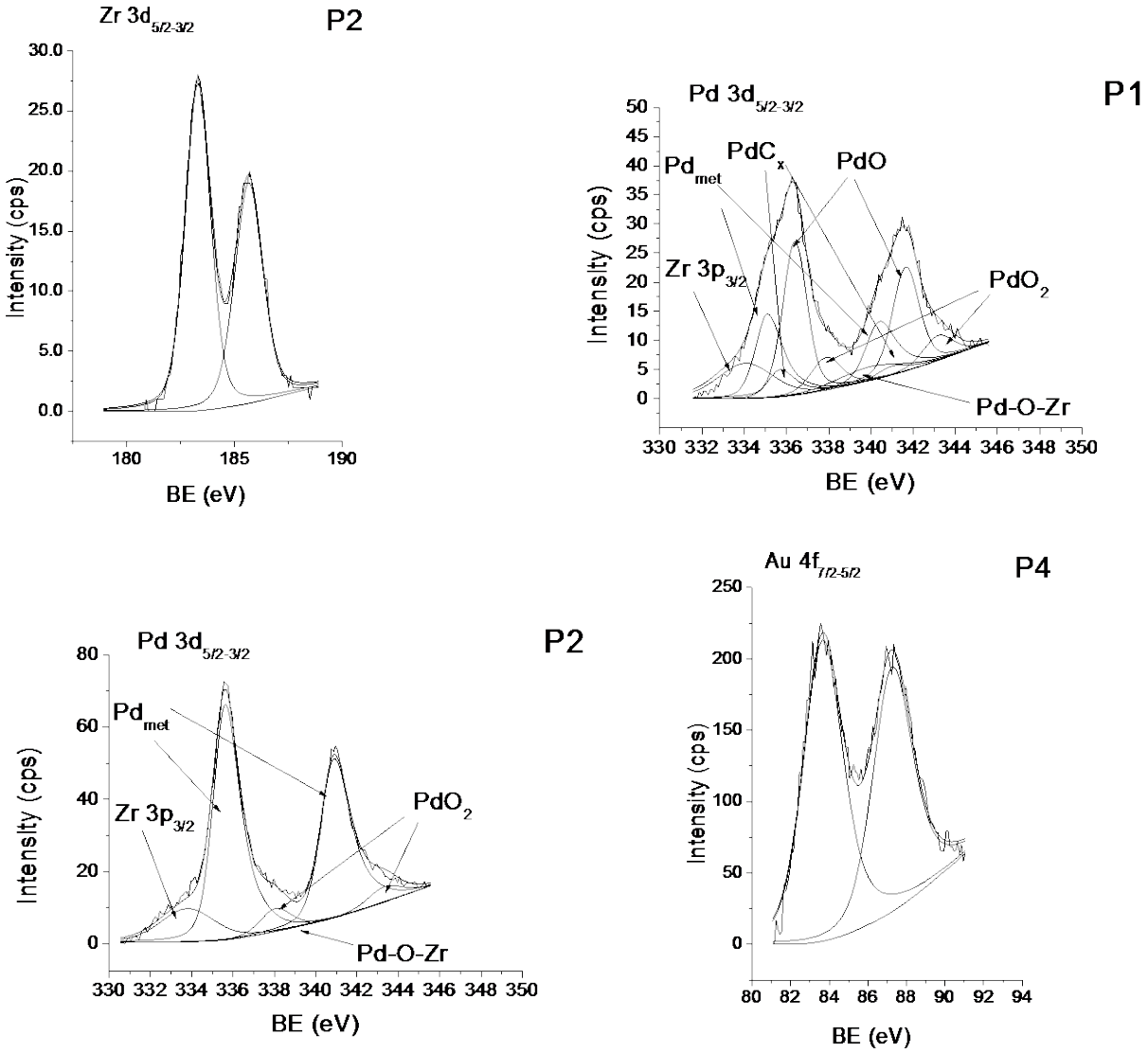

Fig. 4. The exemplary XPS C 1s Zr 3d, Pd 3d and Au 4f spectra fitted to different chemical states using asymmetric Gaussian-Lorentzian functions. The sample notation is taken from the section 2.1.

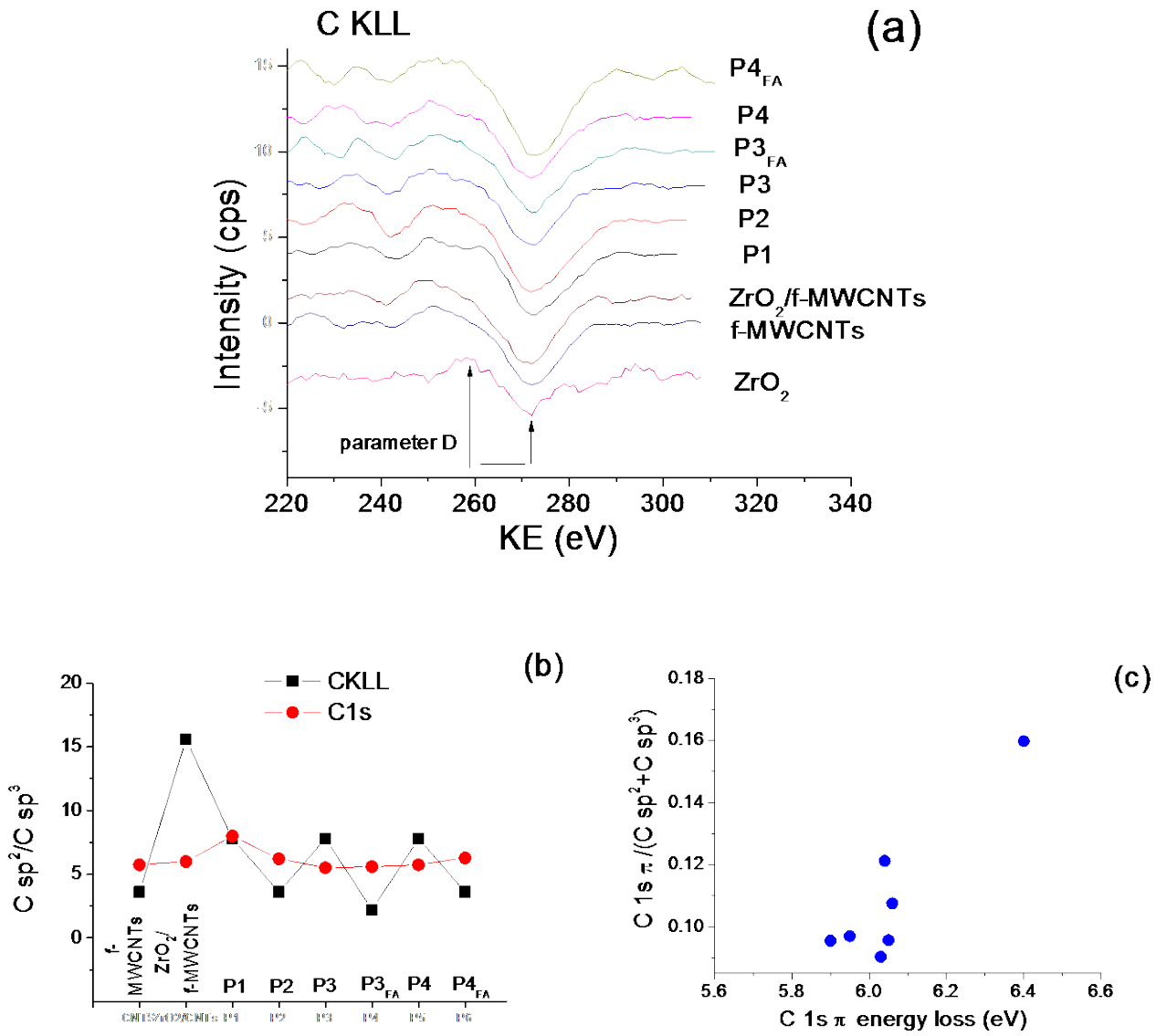

Fig. 5. Comparison of: (a) the first derivative C KLL Auger spectra recorded from the investigated samples, (b) C sp^2/C sp^3 ratio resulting from the fitting of the C 1s spectra (Table 2) and C KLL parameter (assuming a straight line interpolation between 100 C sp^3 – 13.4 eV and 100 sp^2 – 23.1 eV) and (c) ratio of intensity of electron inelastic loss on π bonds to the amount of C sp^2 and sp^3 bonds *versus* electron inelastic energy loss on π bonds. The sample notation is taken from the section 2.1.

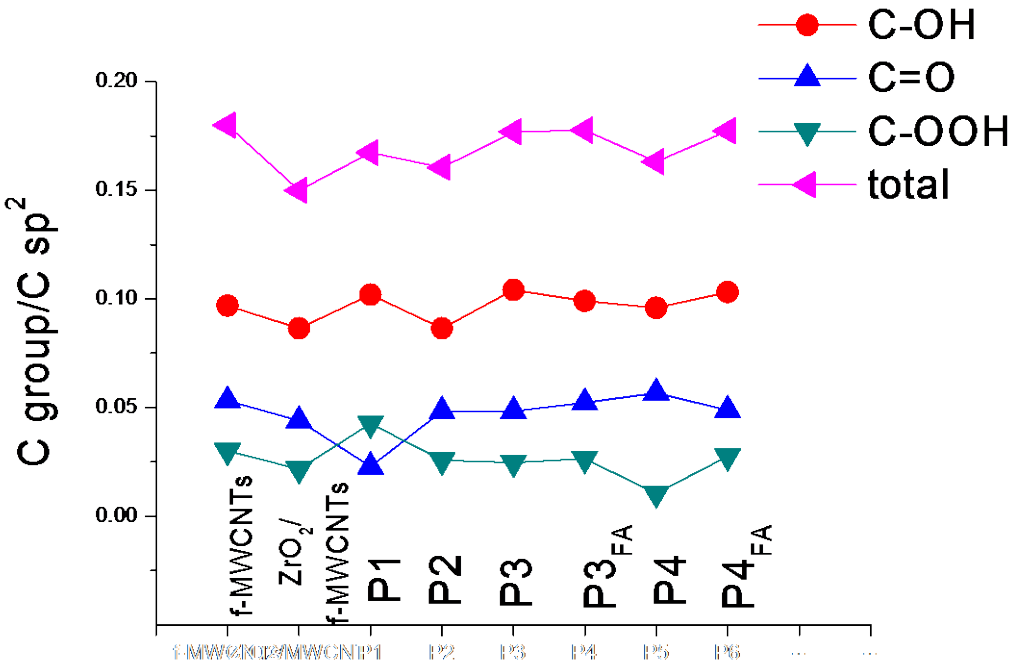

Fig. 6. The ratio of oxygen chemical groups to C sp^2 resulting from the fitting of the XPS C 1s spectra. The sample notation is taken from the section 2.1.

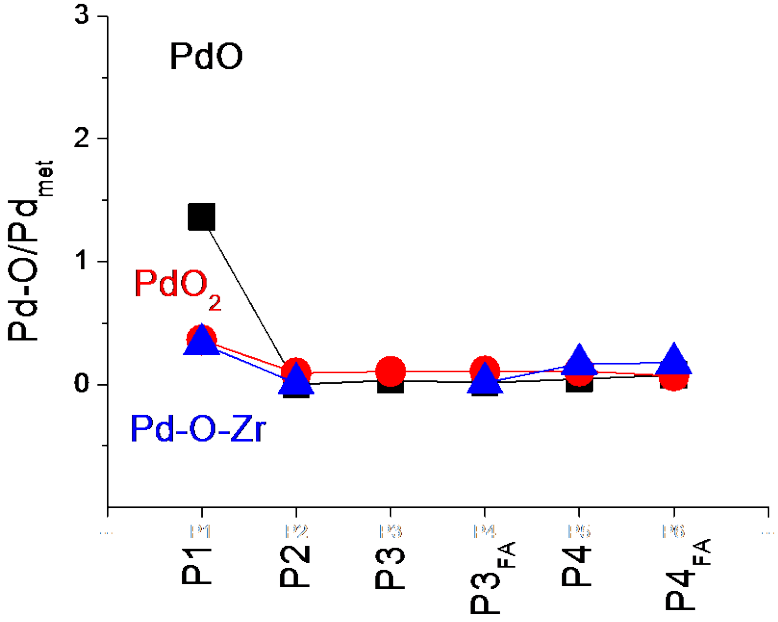

Fig. 7. The ratio of Pd oxides (PdO and PdO_2) and Pd-O-Zr to metallic palladium resulting from the fitting of the XPS Pd 3d spectra. The sample notation is taken from the section 2.1.

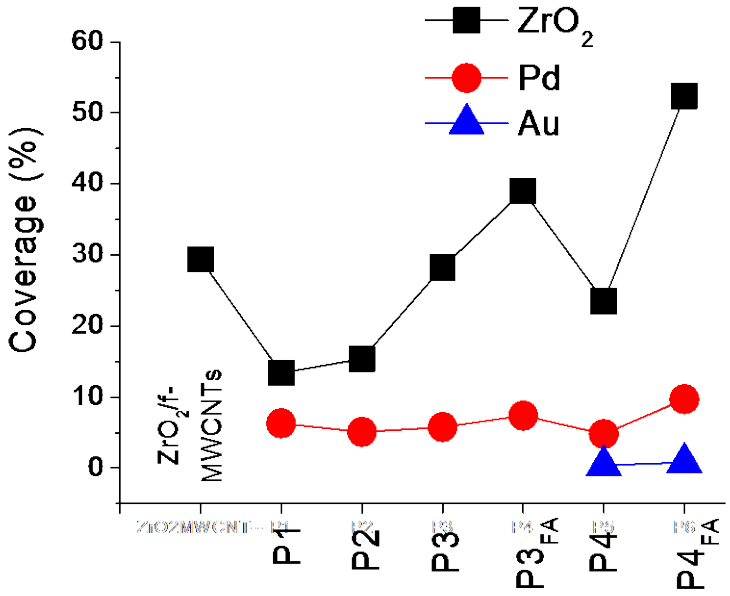

Fig. 8. Coverage of ZrO_2, Pd and Au resulting from evaluation of XPS Zr 3d, Pd 4p and Au 4f spectra using the QUASES analysis.

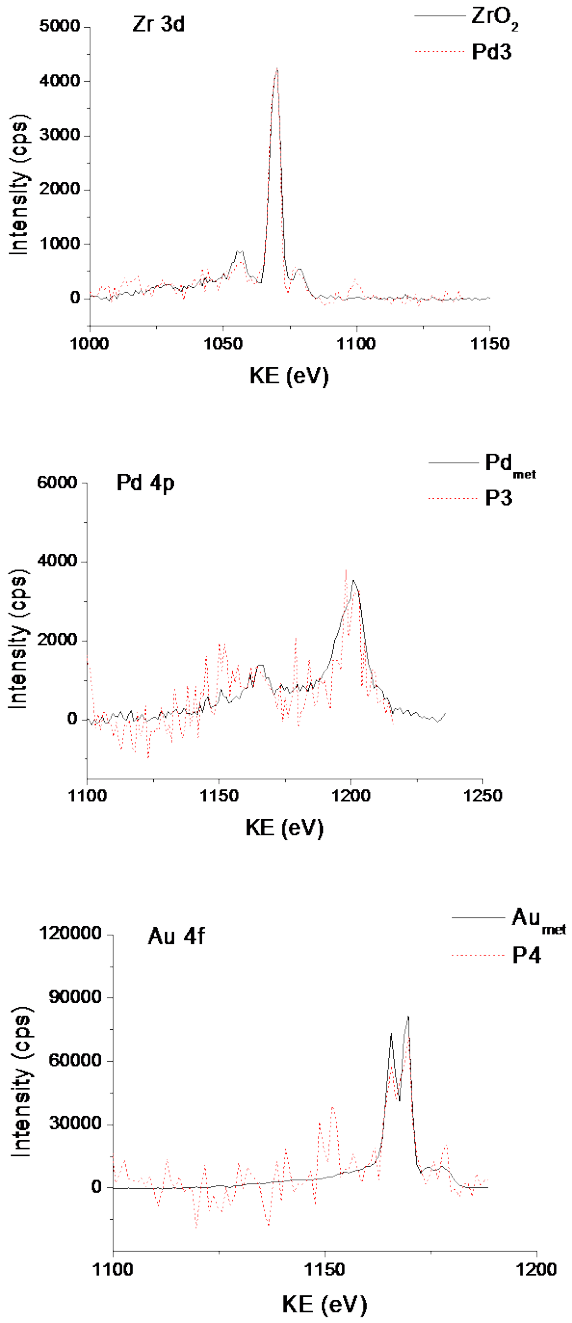

Fig. 9. The results of adjustment of the XPS Zr 3d, Pd 4p and Au 4f spectra recorded from the investigated samples and the standards (ZrO_2 , metallic Pd and Au) for evaluating the ZrO_2, PdAu and Pd/PdAu nanoparticle size using the QUASES-Analyze. The sample notation is taken from the section 2.1.

Suplementary material

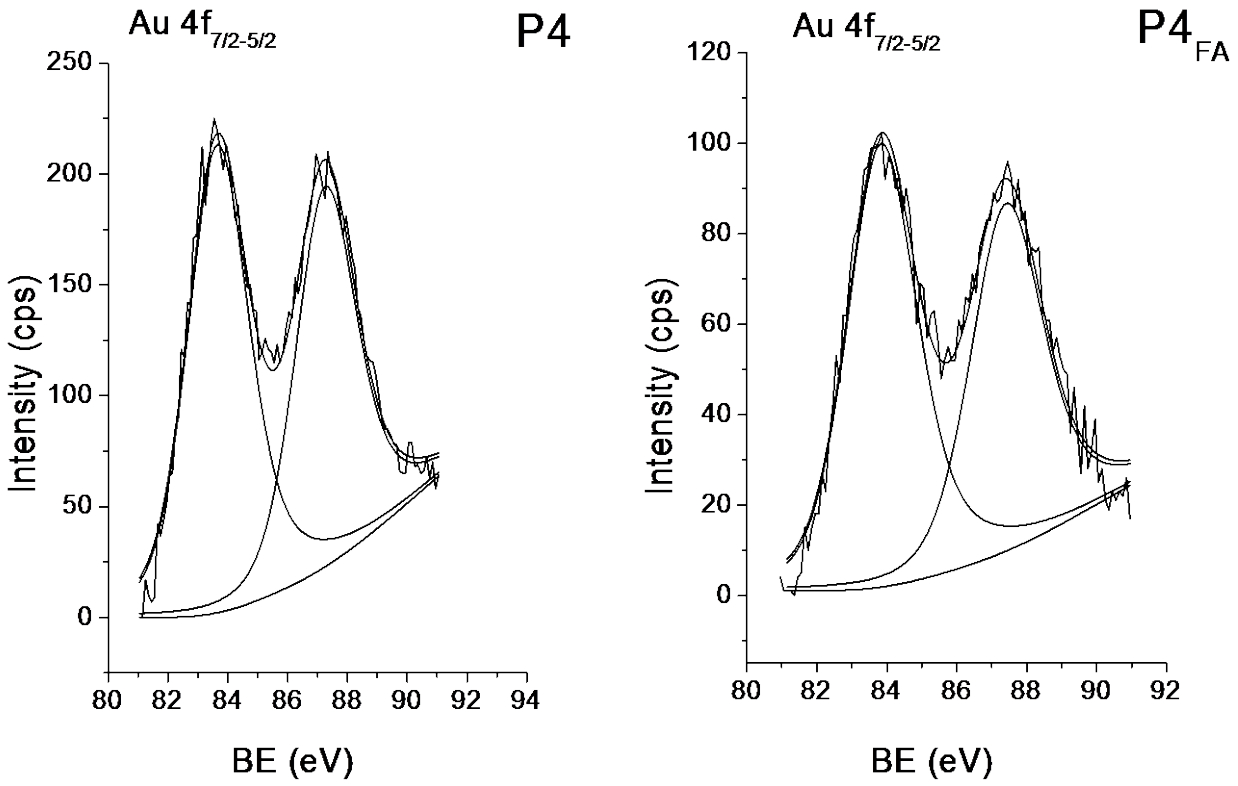

The XPS Au 4f spectra fitted to Gaussian-Lorentzian components.

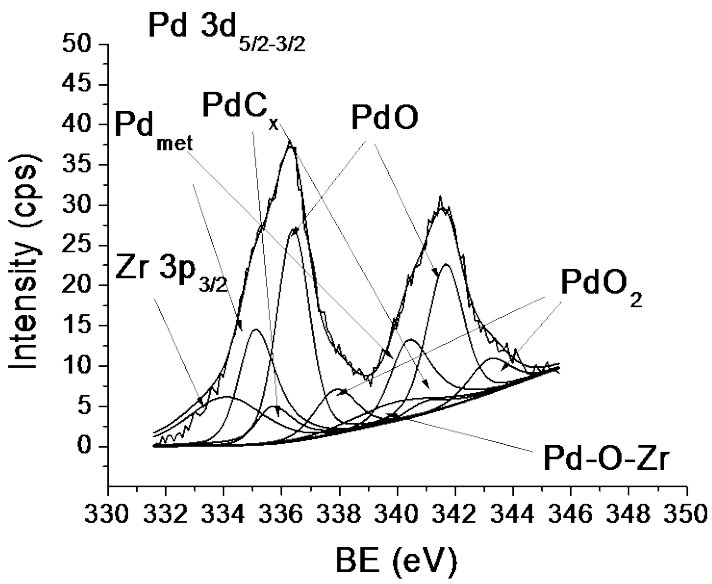

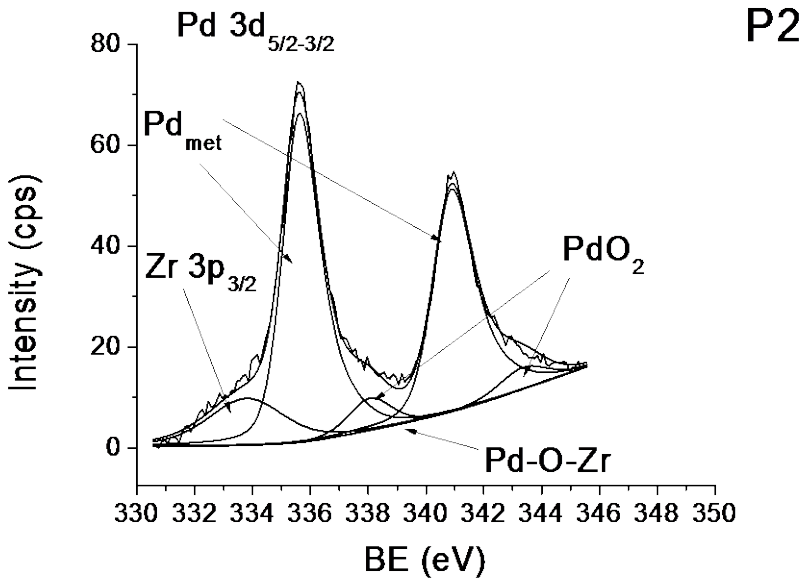

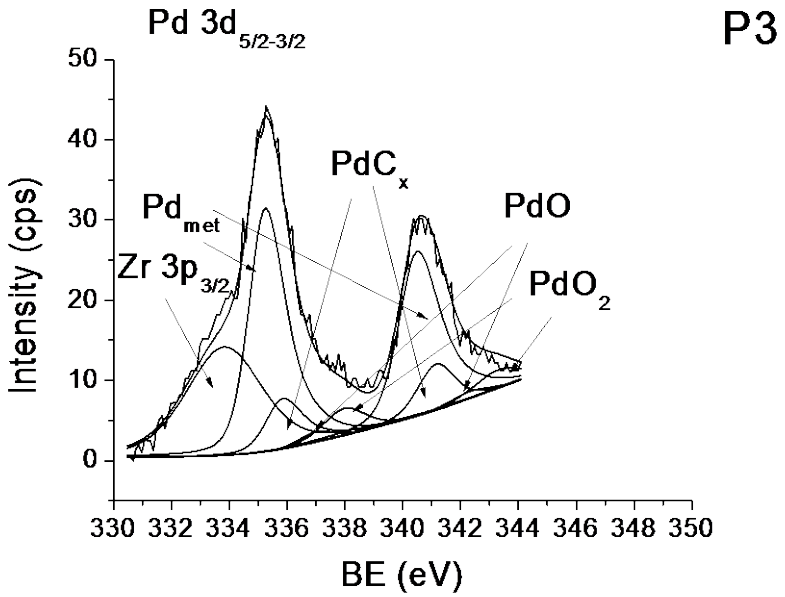

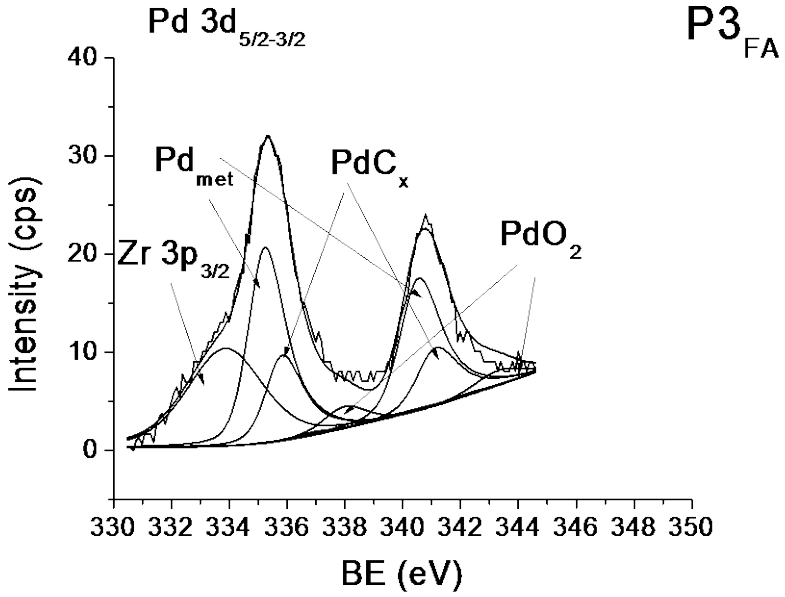

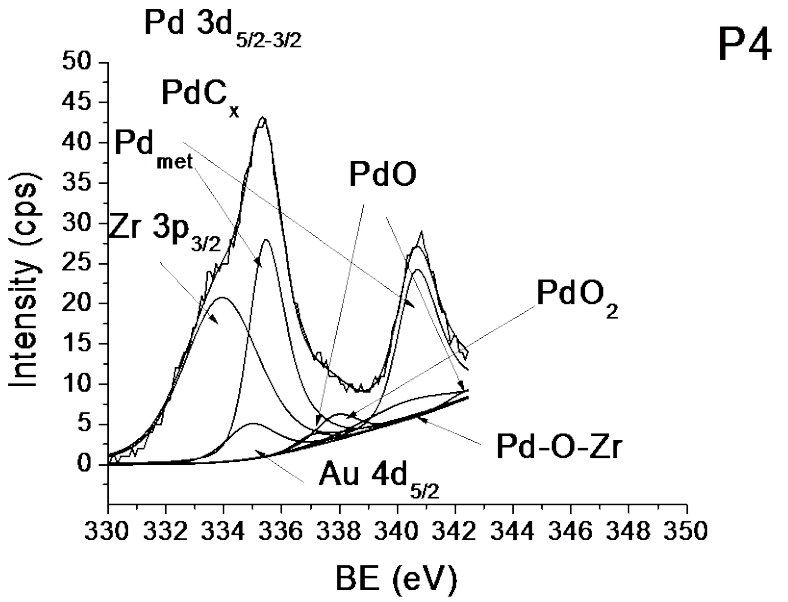

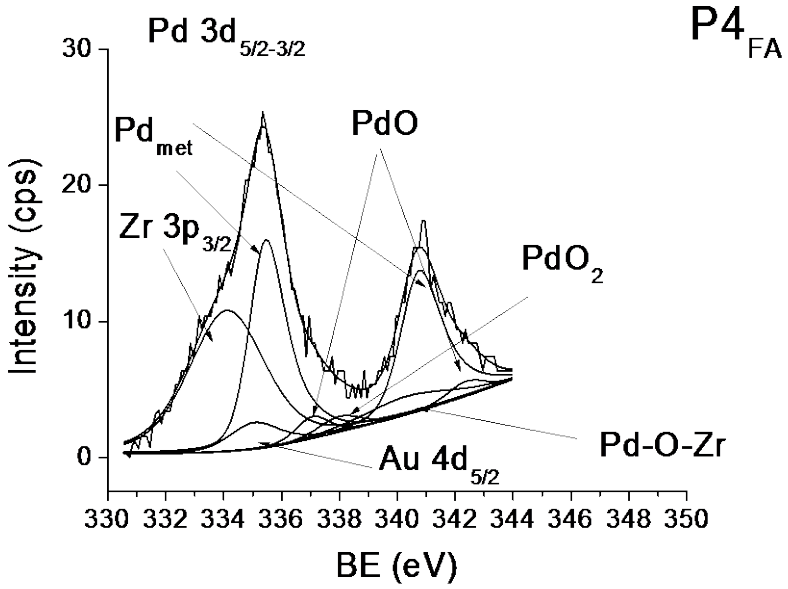

The XPS Pd 3d spectra fitted to Gaussian-Lorentzian components reflecting different Pd chemical states.

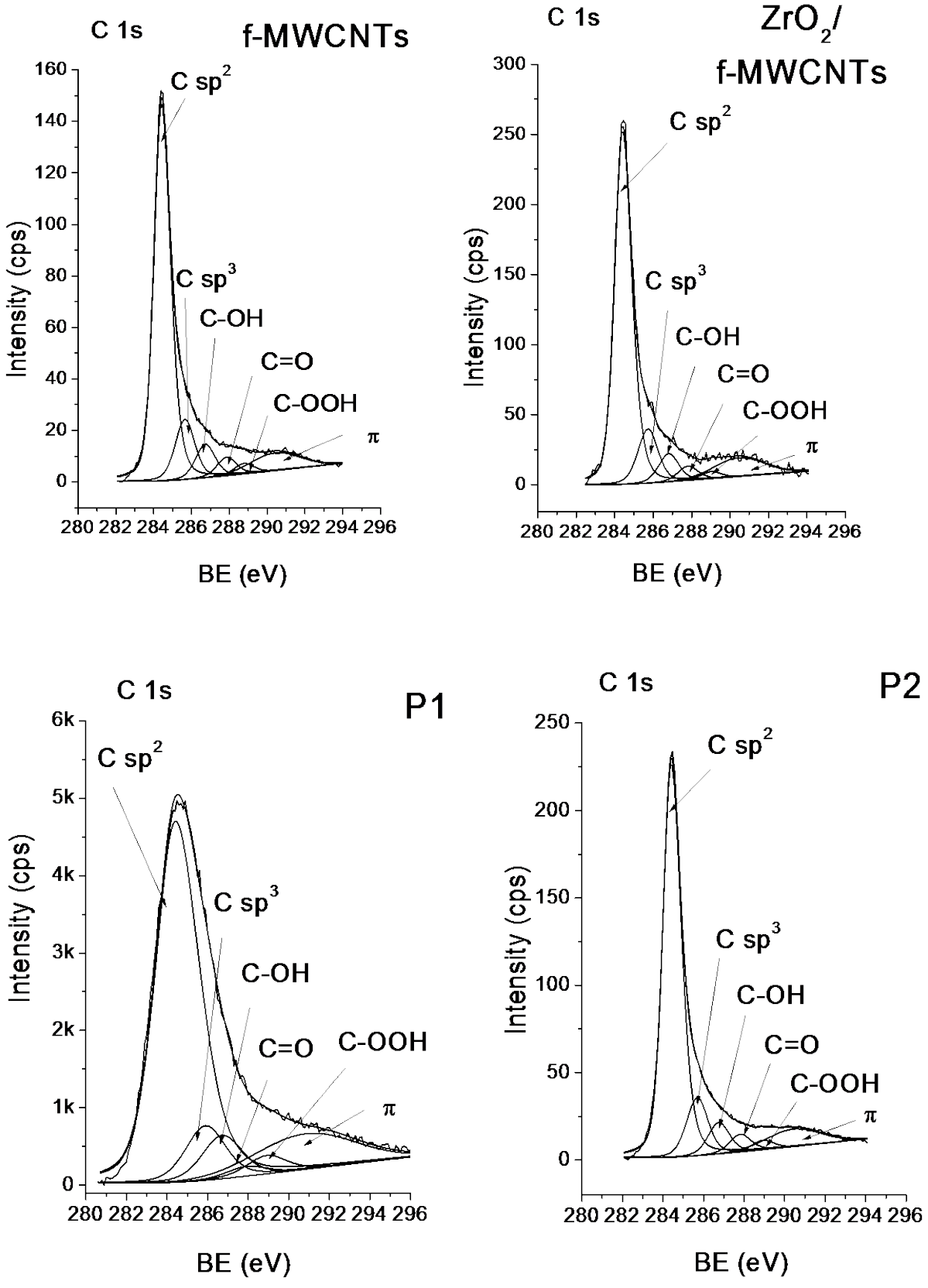

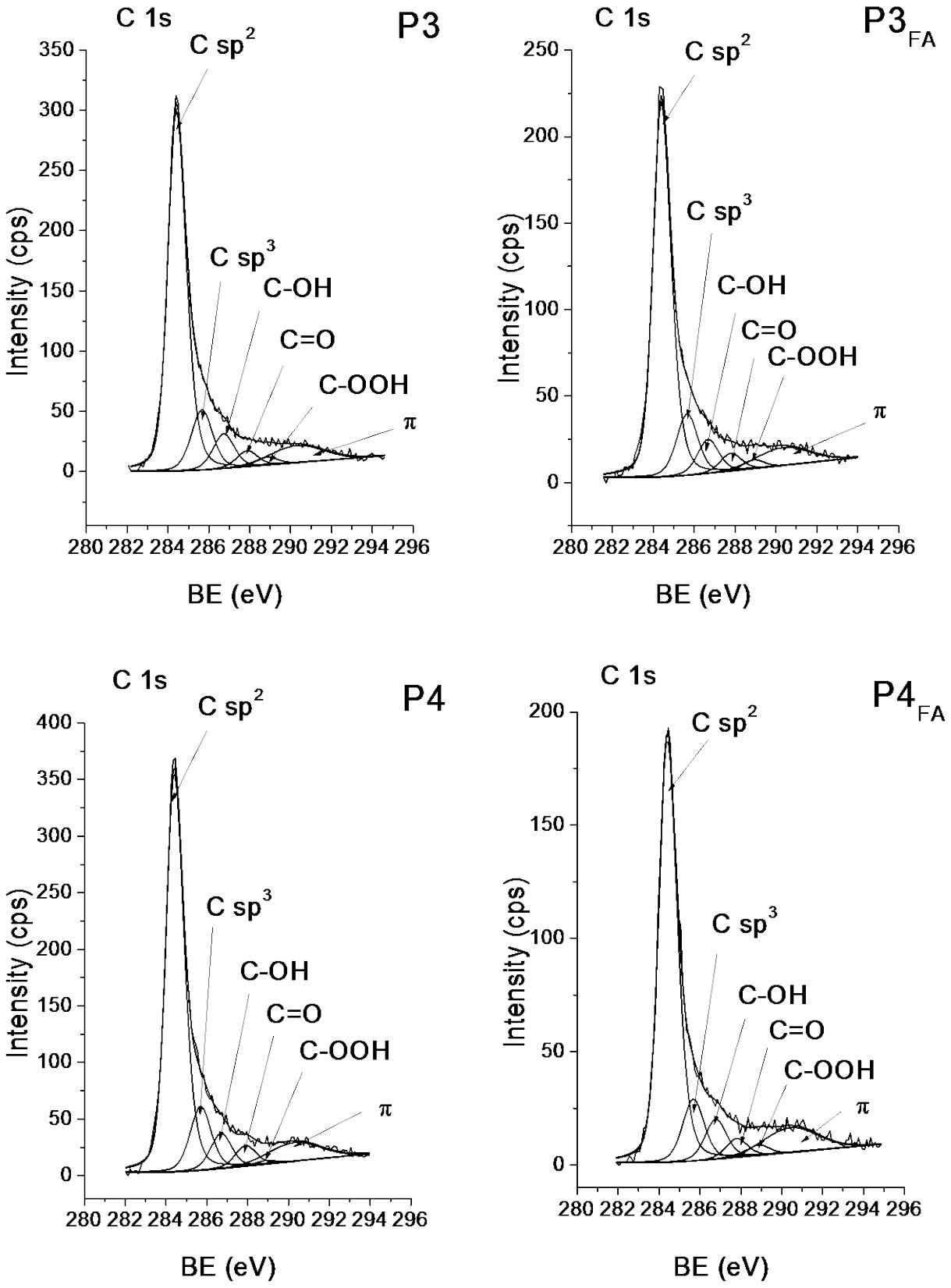

The XPS C 1s spectra fitted to Gaussian-Lorentzian components reflecting different oxygen groups.

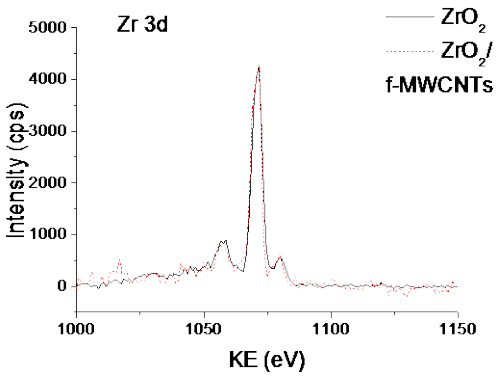

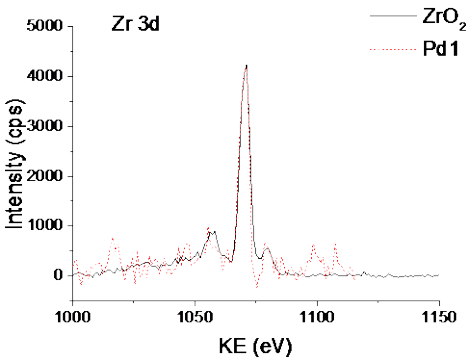

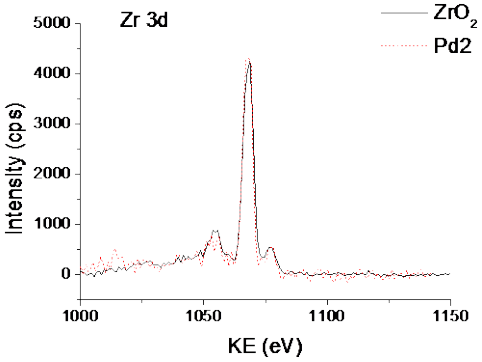

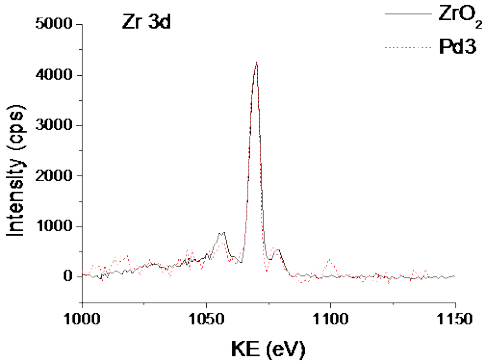

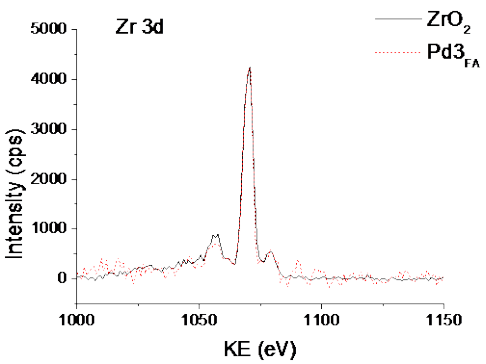

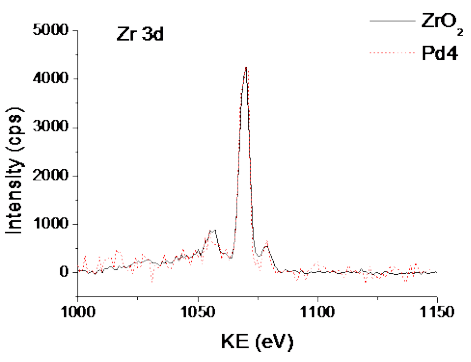

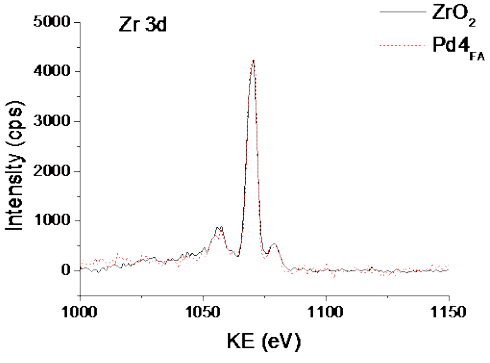

The results of the QUASES-Analyze adjustment of the XPS Zr 3d spectra recorded from the investigated samples to the respective spectrum from the ZrO_2 standard for evaluating ZrO_2 nanoparticle size. The sample notation is taken from the section 2.1.

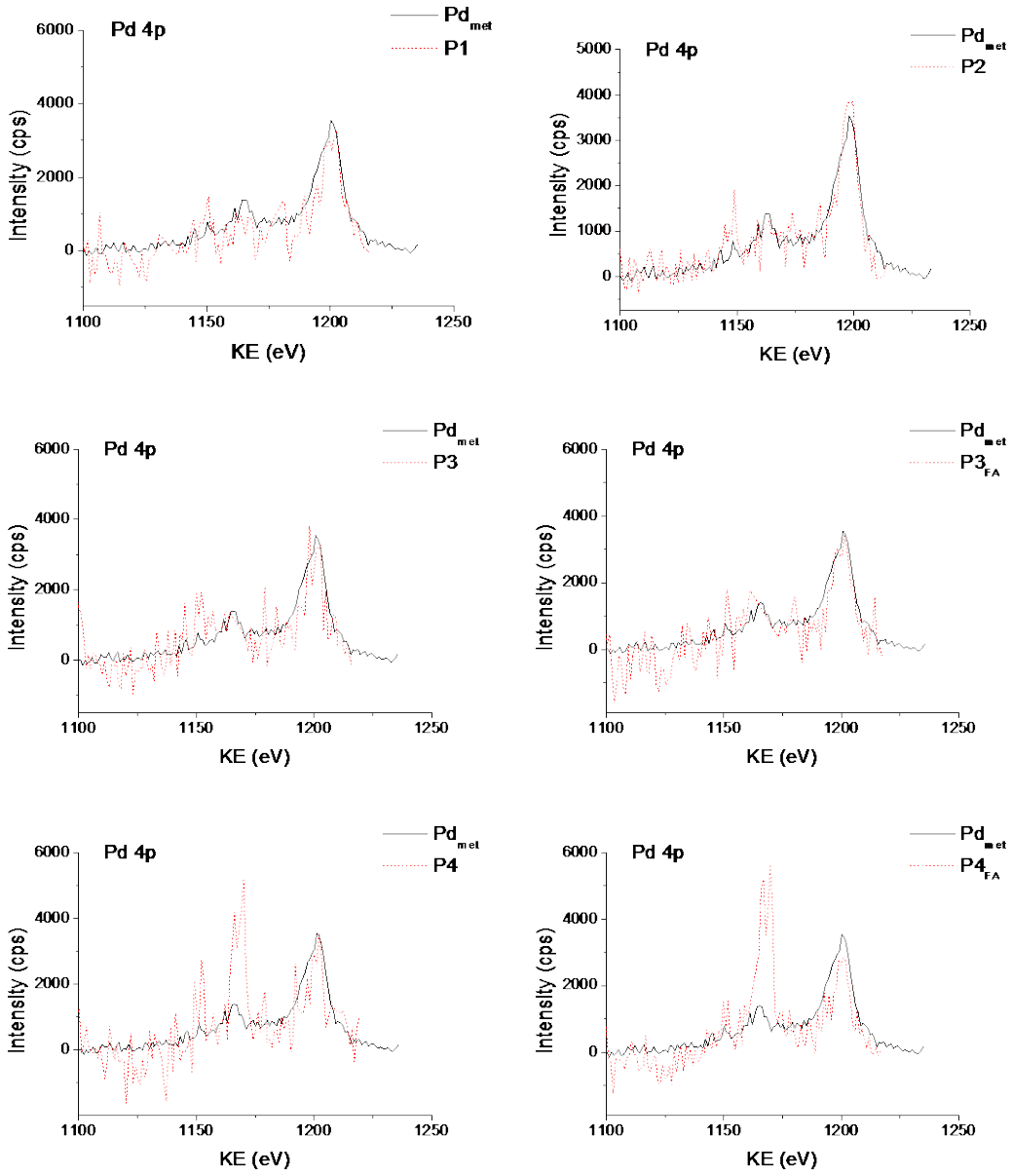

The results of the QUASES-Analyze adjustment of the XPS Pd 4p spectra recorded from the investigated samples to the respective spectrum from and the Pd standard for evaluating the Pd and PdAu nanoparticle size. The sample notation is taken from the section 2.1.

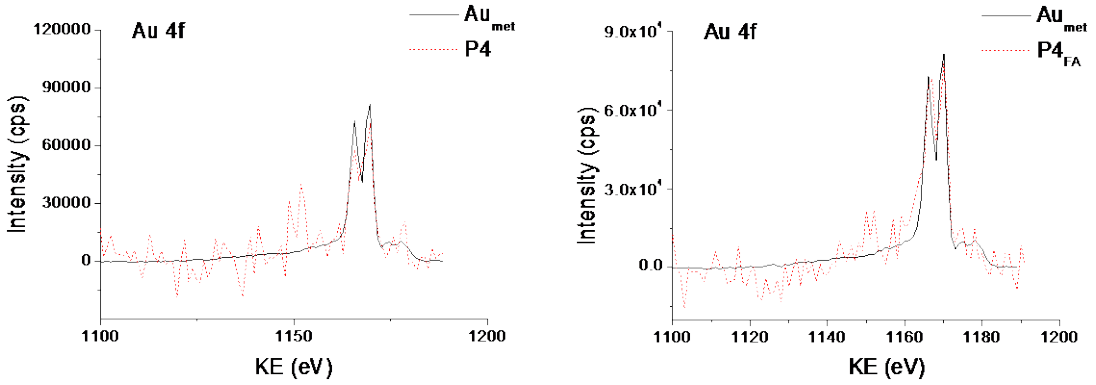

The results of the QUASES-Analyze adjustment of the XPS Au 4f spectra recorded from the investigated samples to the respective spectrum from the Au standard for evaluating the PdAu nanoparticle size. The sample notation is taken from the section 2.1.